Association of Proton Density Fat Fraction in adipose tissue with imaging-based and anthropometric obesity markers in adults

Daniela Franz, MD[1], **Dominik Weidlich, MSc**[1], **Friedemann Freitag**[1], **Christina Holzapfel, PhD**[2], **Theresa Drabsch, MSc**[2], **Thomas Baum, MD**[3], **Holger Eggers, PhD**[4], **Andreas Witte, PhD**[5], **Ernst J. Rummeny, MD**[1], **Hans Hauner, MD**[2], and **Dimitrios C. Karampinos, PhD**[1]

[1]Department of Diagnostic and Interventional Radiology, Klinikum rechts der Isar, Technical University of Munich, Munich, Germany

[2]Institute for Nutritional Medicine, Klinikum rechts der Isar, Technical University of Munich, Munich, Germany

[3]Department of Diagnostic and Interventional Neuroradiology, Klinikum rechts der Isar, Technical University of Munich, Munich, Germany

[4]Philips Research Laboratory, Hamburg, Germany

[5]FOM University of Applied Sciences, Essen, Germany

Abstract

Background/Objectives—The purpose of the present study was to examine the relationship of the proton density fat fraction (PDFF), measured by magnetic resonance imaging (MRI), of supraclavicular and gluteal adipose tissue with subcutaneous and visceral adipose tissue (SAT and VAT) volumes, liver fat fraction and anthropometric obesity markers. The supraclavicular fossa was selected as a typical location where brown adipocytes might be present in humans and the gluteal region was selected as a typical location enclosing primarily white adipocytes.

Subjects/Methods—In this cross-sectional study, 61 adults (44 women, median age 29.3 years, range 21-68 years) underwent an MRI examination of the neck and the abdomen/pelvis (3T, Ingenia, Philips Healthcare). PDFF maps of the supraclavicular and gluteal adipose tissue and the liver were generated. Volumes of SAT and VAT were calculated and supraclavicular and subcutaneous fat were segmented using custom-built post-processing algorithms. Body mass index (BMI), waist circumference and waist-to-height-ratio were recorded. Statistical analysis was conducted using the Student`s t test and Pearson correlation analysis.

Results—Mean supraclavicular PDFF was 75.3 ± 4.7 % *(*range 65.4-83.8 %*)* and mean gluteal PDFF was 89.7 ± 2.9 % (range 82.2-94 %), resulting in a significant difference ($p < 0.0001$).

Corresponding Author: Daniela Franz, MD, Department of Diagnostic and Interventional Radiology, Klinikum rechts der Isar, Technical University of Munich, Ismaninger Str. 22, 81675 Munich, Germany, daniela.franz@tum.de.

Supraclavicular PDFF was positively correlated with VAT (r=0.76, p<0.0001), SAT (r=0.73, p<0.0001), liver PDFF (r=0.42, p=0.0008) and all measured anthropometric obesity markers. Gluteal subcutaneous PDFF also correlated with VAT (r=0.59, p<0.0001), SAT (r=0.63, p<0.0001), liver PDFF (r=0.3, p=0.02) and anthropometric obesity markers.

Conclusions—The positive correlations between adipose tissue PDFF and imaging as well as anthropometric obesity markers suggest that adipose tissue PDFF might be useful as a biomarker for improving the characterization of the obese phenotype, for risk stratification and for selection of appropriate treatment strategies.

Keywords

magnetic resonance imaging (MRI); white fat; brown fat; fat fraction

Introduction

Obesity is linked to various metabolic disturbances and cardiovascular risk factors. This chronic disease represents a leading cause for multi-morbidity and mortality worldwide. There is an urgent need for successful prevention and treatment options based on better phenotyping and risk stratification. The risk implications of obesity are strongly linked to anatomical and functional parameters of adipose tissue (1).

Adipose tissue can be classified based on its histological and functional properties as white, brown or beige (brown-in-white). White adipose tissue (WAT) stores excess energy and possesses several endocrine functions for an extensive inter-organ cross-talk (1). Brown adipose tissue (BAT) is a part of the adipose organ oxidizing glucose and fatty acids via non-shivering thermogenesis for maintenance of body temperature (2–4). BAT can be mostly found in supraclavicular and cervical as well as paravertebral depots in humans, whereas more anatomic sites (e.g., perirenal, mediastinal) have been described to enclose BAT in postmortem studies (5). BAT is an extensively vascularized adipose tissue with large amounts of iron-containing mitochondria, expressing uncoupling protein 1 (UCP-1), a protein uncoupling oxidative phosphorylation from ATP production, thereby releasing energy as heat (2, 3). It is metabolically active mainly throughout early childhood, but it can also be found in adults (5, 6). Recent studies were able to identify a third type of adipose tissue, the "beige" or "brite" phenotype. These studies also suggest that within WAT depots, "browning" can be induced (3). Presumably, beige fat cells are from the same developmental lineage as white adipocytes, while their cell morphology and UCP1-expression resembles those of classical brown adipocytes (3, 7).

Adipose tissue can be further classified based on fat imaging techniques (8). Subcutaneous adipose tissue (SAT) is defined as the layer between the dermis and the aponeuroses and fasciae of the muscles, including mammary adipose tissue. Visceral adipose tissue (VAT) is defined as fat depot within the abdomen, pelvis and within the chest. In the present study, VAT is equivalent to intra-abdominopelvic adipose tissue, according to the classification proposed by Shen et al. (8). Magnetic resonance imaging (MRI)-based phenotyping and quantification of different fat depots has been suggested as a method to improve risk

stratification in persons with obesity and diabetes (9). MRI has been extensively used to quantify the volumes of SAT and VAT (10–12).

An inverse association between the presence of metabolically active BAT and body mass index (BMI) as a measure of body fat mass has been repeatedly shown. For instance lean individuals have more metabolically active BAT than obese subjects (2, 6, 13–15). Studies have also demonstrated an inverse relationship between the presence of metabolically active BAT and visceral fat or WAT in general (15–18). Furthermore, visceral fat was shown to be a central component of the metabolic syndrome and to be closely linked to insulin resistance and consecutive hyperinsulinemia (19–23). Likewise to visceral obesity, BAT was also reported to be inversely related to metabolic risk (13, 17, 24, 25).

At present, Positron Emission Tomography - Computed Tomography (PET/CT) is used as method of choice to demonstrate the presence or absence of functional BAT (13, 15, 26, 27). A main aspect of the PET-based detection of BAT is the dependency of the PET signal on the metabolic activity of adipose tissue, which can be affected by various external factors like outdoor temperature (28, 29).

MRI is a method recently suggested to allow identification of BAT even when not active, without using ionizing radiation (30–33). The most frequently used MRI methods to study human BAT are chemical shift-encoding based fat quantification techniques (34, 35). After consideration of multiple confounding factors, chemical shift encoding-based fat quantification techniques measure the proton density fat fraction (PDFF), which is defined as the proportion of mobile proton density in fat tissue attributable to fat (36). PDFF mapping has recently enabled spatially-resolved fat quantification in multiple organs, and liver PDFF has been emerging as a metabolic phenotyping parameter (37, 38). However, little is known how the PDFF of adipose tissue relates to other fat depots and anthropometric parameters (39, 40).

Therefore, the purpose of the present study was to investigate the relationship of the PDFF of supraclavicular and gluteal adipose tissue with SAT and VAT volumes, liver fat fraction and anthropometric obesity markers. The supraclavicular fossa was selected as a typical location where brown adipocytes might be present in humans and the gluteal region was selected as a typical location enclosing primarily white adipocytes.

Subjects and Methods

Subjects

61 subjects (44 women and 17 men) were recruited at the Institute for Nutritional Medicine, Klinikum rechts der Isar, Technical University of Munich. The subjects had a broad range of BMI (17.4-39.1 kg/m^2). Median age was 29.3 years (range, 21-68). The study protocol was approved by the ethical committee of the Faculty of Medicine of the Technical University of Munich, Germany. Written informed consent was obtained from all subjects prior to phenotyping. Exclusion criteria were severe diseases, pregnancy or lactation, and standard contraindications for MRI examinations.

MRI measurements

Subjects underwent a MRI of the neck and the abdomen/pelvis on a 3T Philips scanner (Ingenia; Philips Healthcare, Best, Netherlands) using a head-neck-coil and a combination of anterior and posterior coil arrays, respectively. Scans were performed at ambient temperature in an air-conditioning-controlled scanner room (21°C) after some acclimatization time, while the study was explained and informed consent was collected.

Supraclavicular and pelvic PDFF mapping—In order to measure the supraclavicular PDFF, MR imaging localizer sequences were first acquired to determine the location of supraclavicular fat pockets. Second, a T1-weighted coronal turbo-spin-echo sequence was acquired for detailed anatomic imaging of the neck. Third, a six-echo multi-echo 3D spoiled gradient echo (six-echo Dixon) sequence was performed axially on the supraclavicular region including the fat pockets. In order to measure gluteal subcutaneous PDFF, localizer sequences were acquired on the abdomen and pelvis, and a six-echo Dixon sequence was performed axially on the posterior side of the upper pelvic region with sequence parameters listed in Table S1. Liver PDFF was measured with a six-echo Dixon sequence axially covering the entire liver in a single breath-hold with sequence parameters listed in Table S1.

All six-echo Dixon sequences used bipolar readout gradients. A small flip angle was employed to minimize T1 bias effects (41, 42). PDFF maps were generated online using a complex-based water-fat separation algorithm, accounting for known confounding factors including phase error correction, a single T2* correction and the consideration of the spectral complexity of fat using the multi-peak fat spectrum model of Ren et al. (43). The multi-peak fat spectrum included fat peaks at spectral locations 0.9 ppm, 1.3 ppm, 1.59 ppm, 2.03 ppm, 2.25 ppm, 2.77 pm and 5.31 ppm, with relative peak amplitudes 62.5 %, 8.5 %, 7.1%, 9.5 %, 6.6 % and 1.6% and 4.2 %, respectively.

SAT/VAT volume measurements—In order to determine the volumes of SAT and VAT, two stacks of axial two-echo Dixon 3D spoiled gradient echo images were acquired for covering the abdomen and the pelvis (border of the upper stack starting at the liver dome). The acquisition time for each two-echo Dixon sequence was 10.6 seconds and each scan was performed in a single breath-hold (sequence parameters listed in Table S1). Water and fat images were separated online on the scanner using the mDixon algorithm (44).

Imaging data analysis

SAT/VAT segmentation—A custom-built post-processing algorithm was used for automatic classification of the different abdominal tissue compartments based on the water-separated and fat-separated images from the two-echo Dixon scan, which has been described extensively in earlier studies (45, 46). SAT, VAT, and non-adipose tissue (water) volumes were determined by summing the segmented regions from the liver dome down to the center of the femoral head. Non-VAT depots (e.g., intermuscular, around spine) were excluded manually slice by slice. In order to account for different body heights, VAT and SAT volumes were standardized by height, resulting in values of ml/cm.

PDFF analysis—For the segmentation of the fat depot in the supraclavicular fossa on the PDFF-maps, an in-house semi-automatic segmentation tool was implemented in Matlab (MathWorks, Natick, MA, USA). The location of the fat depot was defined by one observer by drawing a region of interest (ROI) in one transverse and one coronal slice with inclusion of the entire supraclavicular fossa (fat depot and surrounding tissue) without including any subcutaneous fat. The ROIs were thus confined to the region between the clavicle (inferior border), the trapezius muscle (posterior/lateral border) and the sternocleidomastoid muscle (lateral/anterior border). Voxels with low PDFF values (below 50%) and low T2* values (below 10 ms) were excluded. The threshold of PDFF below 50% was selected empirically in order to exclude muscle regions and the threshold of T2* below 10 ms was selected to exclude regions of trabecularized yellow bone marrow. Smaller isles of connected voxels were excluded, the resulting mask was smoothed and small holes were filled. The above process was performed in order to create a homogenous mask for the supraclavicular fat depot with exclusion of the big vessels, lymph nodes, bone and muscle, resulting in a three-dimensional ROI of the fat depot (Figure S1). The above semi-automatic segmentation process was performed bilaterally. Average PDFF-values of each ROI (in %) were recorded and the average value of both sides was calculated. A similar procedure was performed on the gluteal fat pad posterior of the iliac bone bilaterally, delineating the subcutaneous fat deep to the Scarpa´s fascial layer, excluding gluteal muscles, cutis and vessels.

Liver PDFF was determined by placing three elliptic ROIs into liver segment 6, on the border 6/7 and in segment 7. Mean values of liver PDFF were calculated by averaging the PDFF values in the above three ROIs.

Anthropometric parameter measurements

Waist circumference (WC) was measured as the perimeter midway between the lowest rib margin and the iliac crest on the axial two-echo Dixon water-only images of the abdomen and pelvis, which all were acquired during exhalation. Waist-to-height (WHTR) ratio was then calculated as a ratio of WC (in cm) and height (in cm), whereas height was measured at the nearest 0.5 cm according to standardized operating procedures (SECA, Hamburg, Germany). Weight data are self-reported. BMI was calculated as weight (in kg) divided by height squared (in m^2).

Statistical analysis

Data are expressed as mean ± standard deviation (SD) (with range in parentheses) for normally distributed data, if not otherwise denoted. An unpaired Student´s t test was used to compare the PDFF in the supraclavicular and gluteal adipose tissue. Pearson's correlation analyses were used for normally distributed data. In case the data showed log-normal distributions, logarithmic transformation was performed. Partial correlation analyses were adjusted for age and sex. Statistical analysis was performed using MedCalc Statistical Software (version 16.4.3; MedCalc Software bvba, Ostend, Belgium; https://www.medcalc.org; 2016). A two-sided p-value <0.05 was considered statistically significant and no correction was made for multiple testing due to the explorative character of the study.

To further investigate the effect of age, two age groups were defined according to group size. One group included the subjects with an age younger than 30 years (n=31) and the other group subjects equal to or older than 30 years (n=30). Fisher z-transformation was used for comparing the correlation coefficients.

Results

In total, 61 adults were included in the analysis. Patient characteristics are summarized in Table 1. Standardized volumes of VAT and SAT showed a median of 5.4 ml/cm (range 1.6-39) and 37 ml/cm (range 19.0-143.1), respectively. Median WC was 82 cm (range, 72-119) and median WHTR was 0.49 (range 0.42-0.76). Figure 1 shows representative SAT and VAT color-coded mask, supraclavicular fat PDFF maps and gluteal fat PDFF maps in a female subject with a low BMI (17.4 kg/m^2, age = 39 years) and in another female subject with a high BMI (38.1 kg/m^2, age = 48 years). The subject with obesity is characterized by larger SAT and VAT volumes and higher PDFF values in both the supraclavicular and gluteal fat.

When comparing PDFF in the deep supraclavicular fat pocket to PDFF of the subcutaneous gluteal fat, the mean value was 75.3 ± 4.7 % *(*65.4-83.8) in the supraclavicular fat and 89.7 ± 2.9 % (82.2-94.1) in the subcutaneous gluteal fat, respectively. These values resulted in a significant difference in PDFF between the two fat depots (p<0.0001).

The supraclavicular PDFF was positively correlated with the standardized volumes of both VAT (r=0.76, p<0.0001) and SAT (r=0.73, p<0.0001). When adjusted for age and sex, with age being significantly correlated to all parameters, there was still a strong correlation between the supraclavicular PDFF and the standardized volume of VAT (r=0.73, p<0.0001) and the standardized volume of SAT (r=0.69, p<0.0001), respectively. PDFF in the gluteal subcutaneous fat also showed a strong correlation with VAT volume (r=0.59, p<0.0001; when adjusted for age and sex r=0.70, p<0.0001) as well as with abdominal SAT volume (r=0.63, p<0.0001; when adjusted for age and sex r=0.60, p<0.0001). Correlation analysis of the mean liver PDFF with the supraclavicular PDFF showed a positive correlation of r=0.42 (p=0.0008). The correlation remained statistically significant (r=0.32, p=0.01) after adjustment for age and sex. Gluteal PDFF also showed a correlation with liver PDFF, but less strong compared to supraclavicular PDFF (r=0.3, p=0.02, adjusted for age and sex r=0.29, p=0.02) (Table 2, Figure 2).

PDFF values of both the supraclavicular and gluteal fat were associated with the anthropometric parameters BMI, WC, and WHTR. PDFF of both regions showed significant correlations with the anthropometric parameters also after adjustment for age and sex (Table 3).

When dividing the subjects into two age groups a tendency to stronger associations of all parameters could be observed in the older age group (30 years). Differences between the two age groups were significant for the correlations between supraclavicular PDFF and BMI (p=0.009) and between PDFF and WC (p=0.008) (Table 3). Scatter plots for the older age group are shown in Figure S2.

A multiple regression analysis of supraclavicular PDFF and gluteal PDFF against the anthropometric metrics and imaging makers (VAT, SAT, liver PDFF) was performed to investigate the potential drivers. Results are shown in Table S2.

Discussion

The present study shows a significant evidence of a difference between the PDFF in the supraclavicular and gluteal fat depots, pointing towards a difference in cellular characteristics between the two locations. Furthermore, PDFF of the analyzed adipose tissue depots was closely correlated to both MR-based and anthropometric markers of obesity and the liver fat fraction.

The recent re-discovery of the presence of BAT in adults has incited interest to search for innocuous methods to detect BAT and to learn more about the presence and function of BAT, as animal studies have suggested a role of BAT in metabolic health, particularly in the context of obesity and type 2 diabetes.

The results of the present study showing a PDFF in supraclavicular adipose tissue of 75.3 ± 4.7 % and in subcutaneous gluteal adipose tissue of 89.7 ± 2.9 % are in line with results from recent studies, revealing a significant evidence for a difference between deep supraclavicular and subcutaneous adipose tissue (31, 34, 40, 47, 48). The lower PDFF in the supraclavicular region may indicate a lower fat content. It is plausible to speculate that the presence of brown and beige fat cells may be responsible for this difference (30). The supraclavicular fat depot is the most prominent region in humans, for which PET/CT scans have detected activated BAT (2, 49). The detection of BAT in individual adults varies largely and ranges from 20 to 96 % depending on age, BMI and methodological approach (6, 50). Brown and beige fat cells are known to have lower lipid content and more mitochondria providing a plausible explanation for the difference in PDFF. However, there are other potential reasons for this difference such as white fat cell size, vascularization and contamination by other cell types including immune cells (51). The values reported for supraclavicular PDFF lie between the ranges of MRI-based fat fraction values previously found in neonates and children and those found in the elderly (35, 39, 47). The underlying hypothesis is that the amount of BAT decreases with ageing, and the supraclavicular fat compartment more and more resembles a white-fat compartment like the subcutaneous compartment (28).

Furthermore, our analyses revealed a positive association between the supraclavicular PDFF and several anthropometric obesity markers (BMI, WC, WHTR) as well as liver fat fraction and volumes of SAT and VAT. If the supraclavicular fat depot is considered as a depot containing largely brown fat cells this finding is in line with data from PET/CT studies which have shown lower BMI being associated with more activated BAT (13, 28). Several studies also found correlations between the presence of metabolically active BAT using PET/CT and the amount of visceral fat and subcutaneous fat with a higher prevalence of metabolically active BAT in subjects with lower amounts of SAT and VAT (15–18, 25, 27).

Recent studies measuring BAT triglyceride content determined by single-voxel proton magnetic resonance spectroscopy found a positive correlation with BMI and WC as well as subcutaneous and visceral fat masses (52, 53). Another recent study revealed a correlation between MRI-determined BAT characteristics in supraclavicular adipose tissue and metabolic and obesity markers, showing lower triglyceride levels, lower WC and absence of metabolic syndrome and type 2 diabetes in subjects with BAT presence, as measured by a higher MRI-fat fraction difference between supraclavicular and subcutaneous adipose tissue (39). A tempting explanation is that with growing BMI brown adipocytes are to some extent replaced by white adipocytes reflecting a kind of "whitening" in this specific fat depot, a process resulting from vascular rarefaction and dysfunction (54). A definite answer would require a histological and functional analysis using adipose tissue biopsies.

Regarding the correlation of supraclavicular PDFF with liver PDFF, Bartelt et al. showed the influence of metabolically active BAT on triglyceride clearance in mice, with cold exposure shifting the clearance of lipo-proteins from liver to BAT (55). This is potentially in line with the results of the present study with liver PDFF being positively correlated with supraclavicular PDFF, i.e. supposedly less supraclavicular BAT, reflected by a higher PDFF, being correlated with higher liver fat values. It has to be noted that no association between subcutaneous PDFF and liver fat was found suggesting that expansion of this specific fat depot is not linked to an unhealthy metabolic phenotype. It has to be further studied whether there is an influence of metabolically active BAT on triglyceride clearance in humans.

In subjects older than 30 years, the associations found in the present study were even stronger than in subjects in their 20s. Yoneshiro et al. showed that adiposity-related parameters (e.g., visceral fat area, BMI) increased with age in subjects without active BAT, while they remained unchanged in subjects with active BAT. This might suggest a protective role of BAT against the aging-related accumulation of body fat (26).

The present study also revealed positive correlations of PDFF in gluteal subcutaneous fat, thus WAT, with BMI, WC and WHTR as well as volumes of SAT and VAT and liver fat. Those correlations may be simply explained by fat cell hypertrophy which is a characteristic feature of weight gain which may result in a proportional increase in the overall fat content (56). However, Yang et al. could not find a correlation between adipocyte cell size and chemical-shift measured fat fraction (57). Nevertheless, PDFF of a tissue may be influenced by its vascularity, as adipocyte hypertrophy is known to be related to a rarefaction of capillaries and reduction of angiogenic potential (58). Irrespective of the underlying mechanisms, these associations are also consistent with previous findings relating CT-based SAT attenuation to obesity markers, revealing a correlation of lower CT-attenuation (i.e., higher fat content) of adipose tissue with higher BMI, WC, incidence of cardiovascular disease and a profile of biomarkers suggestive of greater metabolic risk (59–62).

Limitations

The present study has some limitations. First, histology was not used as a gold standard diagnostic tool in differentiating WAT from BAT. Without adipose tissue biopsy samples, it is not possible to ultimately substantiate the presence of BAT as well as the cellular characteristics of the depots under investigation. Second, when performing PDFF

measurements with MRI, partial volume effects have to be taken into account. PDFF cannot differentiate between intracellular water content and non-lipid tissue portions (e.g., from vessels) within a voxel. The isotropic voxel size in our study was 1.5 mm large in each dimension, thus partial volume effects from very small vessels and adjacent muscles cannot be excluded. Furthermore, PDFF cannot discriminate between a cluster of brown adipocytes and mixed clusters of white and brown adipocytes, giving only average values of volumes of interest. For calculation of the BMI, self-reported weight data was used, which may have led to minor inaccuracies. Finally, single-voxel MR spectroscopy was not performed to verify the reported PDFF differences in gluteal fat.

In conclusion, this study shows a significant difference between supraclavicular and subcutaneous PDFF, pointing towards BAT being present in the supraclavicular fat depot in adults. Furthermore, PDFF values of the two analyzed adipose tissue depots are correlated to both MR-based and anthropometric markers of obesity. The correlation of supraclavicular PDFF with obesity markers is in line with the assumed relationship between BAT and obesity. The correlation of the subcutaneous PDFF with obesity markers is consistent with previous findings relating CT-based SAT attenuation to obesity markers. Consequently, the present findings suggest that adipose tissue PDFF can not only identify the presence of BAT in the supraclavicular adipose tissue, but might also be used as biomarker in SAT for improving the characterization of the obese phenotype, for risk stratification and for selection of appropriate treatment and lifestyle interventions in the future.

Supplementary Material

Refer to Web version on PubMed Central for supplementary material.

Acknowledgements

References

1. Rosen ED, Spiegelman BM. What we talk about when we talk about fat. Cell. 2014; 156(1–2):20–44. DOI: 10.1016/j.cell.2013.12.012 [PubMed: 24439368]

2. Cypess AM, Lehman S, Williams G, Tal I, Rodman D, Goldfine AB, et al. Identification and importance of brown adipose tissue in adult humans. N Engl J Med. 2009; 360(15):1509–17. DOI: 10.1056/NEJMoa0810780 [PubMed: 19357406]

3. Harms M, Seale P. Brown and beige fat: development, function and therapeutic potential. Nat Med. 2013; 19(10):1252–63. DOI: 10.1038/nm.3361 [PubMed: 24100998]

4. Cannon B, Nedergaard J. Brown adipose tissue: function and physiological significance. Physiol Rev. 2004; 84(1):277–359. DOI: 10.1152/physrev.00015.2003 [PubMed: 14715917]

5. Heaton JM. The distribution of brown adipose tissue in the human. J Anat. 1972; 112(Pt 1):35–9. [PubMed: 5086212]

6. van Marken Lichtenbelt WD, Vanhommerig JW, Smulders NM, Drossaerts JM, Kemerink GJ, Bouvy ND, et al. Cold-activated brown adipose tissue in healthy men. N Engl J Med. 2009; 360(15):1500–8. DOI: 10.1056/NEJMoa0808718 [PubMed: 19357405]

7. Wu J, Bostrom P, Sparks LM, Ye L, Choi JH, Giang AH, et al. Beige adipocytes are a distinct type of thermogenic fat cell in mouse and human. Cell. 2012; 150(2):366–76. DOI: 10.1016/j.cell. 2012.05.016 [PubMed: 22796012]

8. Shen W, Wang Z, Punyanita M, Lei J, Sinav A, Kral JG, et al. Adipose tissue quantification by imaging methods: a proposed classification. Obes Res. 2003; 11(1):5–16. DOI: 10.1038/oby.2003.3 [PubMed: 12529479]

9. Thomas EL, Parkinson JR, Frost GS, Goldstone AP, Dore CJ, McCarthy JP, et al. The missing risk: MRI and MRS phenotyping of abdominal adiposity and ectopic fat. Obesity (Silver Spring). 2012; 20(1):76–87. DOI: 10.1038/oby.2011.142 [PubMed: 21660078]

10. Machann J, Thamer C, Stefan N, Schwenzer NF, Kantartzis K, Haring HU, et al. Follow-up whole-body assessment of adipose tissue compartments during a lifestyle intervention in a large cohort at increased risk for type 2 diabetes. Radiology. 2010; 257(2):353–63. DOI: 10.1148/radiol. 10092284 [PubMed: 20713612]

11. Machann J, Thamer C, Schnoedt B, Haap M, Haring HU, Claussen CD, et al. Standardized assessment of whole body adipose tissue topography by MRI. J Magn Reson Imaging. 2005; 21(4):455–62. DOI: 10.1002/jmri.20292 [PubMed: 15778954]

12. Klopfenstein BJ, Kim MS, Krisky CM, Szumowski J, Rooney WD, Purnell JQ. Comparison of 3 T MRI and CT for the measurement of visceral and subcutaneous adipose tissue in humans. Br J Radiol. 2012; 85(1018):e826–30. DOI: 10.1259/bjr/57987644 [PubMed: 22514099]

13. Saito M, Okamatsu-Ogura Y, Matsushita M, Watanabe K, Yoneshiro T, Nio-Kobayashi J, et al. High incidence of metabolically active brown adipose tissue in healthy adult humans: effects of cold exposure and adiposity. Diabetes. 2009; 58(7):1526–31. DOI: 10.2337/db09-0530 [PubMed: 19401428]

14. Lee P, Greenfield JR, Ho KK, Fulham MJ. A critical appraisal of the prevalence and metabolic significance of brown adipose tissue in adult humans. Am J Physiol Endocrinol Metab. 2010; 299(4):E601–6. DOI: 10.1152/ajpendo.00298.2010 [PubMed: 20606075]

15. Matsushita M, Yoneshiro T, Aita S, Kameya T, Sugie H, Saito M. Impact of brown adipose tissue on body fatness and glucose metabolism in healthy humans. Int J Obes (Lond). 2014; 38(6):812–7. DOI: 10.1038/ijo.2013.206 [PubMed: 24213309]

16. Green A, Bagci U, Kelly P, Osman M. Brown adipose tissue detected by FDG PET/CT is associated with less central abdominal visceral fat. Journal of Nuclear Medicine. 2015; 56(3)

17. Chalfant JS, Smith ML, Hu HH, Dorey FJ, Goodarzian F, Fu CH, et al. Inverse association between brown adipose tissue activation and white adipose tissue accumulation in successfully treated pediatric malignancy. Am J Clin Nutr. 2012; 95(5):1144–9. DOI: 10.3945/ajcn.111.030650 [PubMed: 22456659]

18. Cronin CG, Prakash P, Daniels GH, Boland GW, Kalra MK, Halpern EF, et al. Brown fat at PET/CT: correlation with patient characteristics. Radiology. 2012; 263(3):836–42. DOI: 10.1148/radiol.12100683 [PubMed: 22623697]

19. Wajchenberg BL. Subcutaneous and visceral adipose tissue: their relation to the metabolic syndrome. Endocr Rev. 2000; 21(6):697–738. DOI: 10.1210/edrv.21.6.0415 [PubMed: 11133069]

20. Larsson B, Svardsudd K, Welin L, Wilhelmsen L, Bjorntorp P, Tibblin G. Abdominal adipose tissue distribution, obesity, and risk of cardiovascular disease and death: 13 year follow up of participants in the study of men born in 1913. Br Med J (Clin Res Ed). 1984; 288(6428):1401–4.

21. Blair D, Habicht JP, Sims EA, Sylwester D, Abraham S. Evidence for an increased risk for hypertension with centrally located body fat and the effect of race and sex on this risk. Am J Epidemiol. 1984; 119(4):526–40. [PubMed: 6711542]

22. Fox CS, Massaro JM, Hoffmann U, Pou KM, Maurovich-Horvat P, Liu CY, et al. Abdominal visceral and subcutaneous adipose tissue compartments: association with metabolic risk factors in the Framingham Heart Study. Circulation. 2007; 116(1):39–48. DOI: 10.1161/CIRCULATIONAHA.106.675355 [PubMed: 17576866]

23. Abraham TM, Pedley A, Massaro JM, Hoffmann U, Fox CS. Association between visceral and subcutaneous adipose depots and incident cardiovascular disease risk factors. Circulation. 2015; 132(17):1639–47. DOI: 10.1161/CIRCULATIONAHA.114.015000 [PubMed: 26294660]

24. Coelho MS, de Lima CL, Royer C, Silva JB, Oliveira FC, Christ CG, et al. GQ-16, a TZD-Derived Partial PPARgamma Agonist, Induces the Expression of Thermogenesis-Related Genes in Brown Fat and Visceral White Fat and Decreases Visceral Adiposity in Obese and Hyperglycemic Mice. PLoS One. 2016; 11(5):e0154310.doi: 10.1371/journal.pone.0154310 [PubMed: 27138164]

25. Wang Q, Zhang M, Xu M, Gu W, Xi Y, Qi L, et al. Brown adipose tissue activation is inversely related to central obesity and metabolic parameters in adult human. PLoS One. 2015; 10(4):e0123795.doi: 10.1371/journal.pone.0123795 [PubMed: 25894250]

26. Yoneshiro T, Aita S, Matsushita M, Okamatsu-Ogura Y, Kameya T, Kawai Y, et al. Age-related decrease in cold-activated brown adipose tissue and accumulation of body fat in healthy humans. Obesity (Silver Spring). 2011; 19(9):1755–60. DOI: 10.1038/oby.2011.125 [PubMed: 21566561]

27. Wang Q, Zhang M, Ning G, Gu W, Su T, Xu M, et al. Brown adipose tissue in humans is activated by elevated plasma catecholamines levels and is inversely related to central obesity. PLoS One. 2011; 6(6):e21006.doi: 10.1371/journal.pone.0021006 [PubMed: 21701596]

28. Ouellet V, Routhier-Labadie A, Bellemare W, Lakhal-Chaieb L, Turcotte E, Carpentier AC, et al. Outdoor temperature, age, sex, body mass index, and diabetic status determine the prevalence, mass, and glucose-uptake activity of 18F-FDG-detected BAT in humans. J Clin Endocrinol Metab. 2011; 96(1):192–9. DOI: 10.1210/jc.2010-0989 [PubMed: 20943785]

29. Sampath SC, Sampath SC, Bredella MA, Cypess AM, Torriani M. Imaging of Brown Adipose Tissue: State of the Art. Radiology. 2016; 280(1):4–19. DOI: 10.1148/radiol.2016150390 [PubMed: 27322970]

30. Gifford A, Towse TF, Walker RC, Avison MJ, Welch EB. Characterizing active and inactive brown adipose tissue in adult humans using PET-CT and MR imaging. Am J Physiol Endocrinol Metab. 2016; 311(1):E95–E104. DOI: 10.1152/ajpendo.00482.2015 [PubMed: 27166284]

31. Stahl V, Maier F, Freitag MT, Floca RO, Berger MC, Umathum R, et al. In vivo assessment of cold stimulation effects on the fat fraction of brown adipose tissue using DIXON MRI. J Magn Reson Imaging. 2017; 45(2):369–80. DOI: 10.1002/jmri.25364 [PubMed: 27421080]

32. Gifford A, Towse TF, Walker RC, Avison MJ, Welch EB. Human brown adipose tissue depots automatically segmented by positron emission tomography/computed tomography and registered magnetic resonance images. J Vis Exp. 2015; (96)doi: 10.3791/52415

33. van Rooijen BD, van der Lans AA, Brans B, Wildberger JE, Mottaghy FM, Schrauwen P, et al. Imaging cold-activated brown adipose tissue using dynamic T2*-weighted magnetic resonance imaging and 2-deoxy-2-[18F]fluoro-D-glucose positron emission tomography. Invest Radiol. 2013; 48(10):708–14. DOI: 10.1097/RLI.0b013e31829363b8 [PubMed: 23695084]

34. Hu HH, Yin L, Aggabao PC, Perkins TG, Chia JM, Gilsanz V. Comparison of brown and white adipose tissues in infants and children with chemical-shift-encoded water-fat MRI. J Magn Reson Imaging. 2013; 38(4):885–96. DOI: 10.1002/jmri.24053 [PubMed: 23440739]

35. Rasmussen JM, Entringer S, Nguyen A, van Erp TG, Burns J, Guijarro A, et al. Brown adipose tissue quantification in human neonates using water-fat separated MRI. PLoS One. 2013; 8(10):e77907.doi: 10.1371/journal.pone.0077907 [PubMed: 24205024]

36. Reeder SB, Hu HH, Sirlin CB. Proton density fat-fraction: a standardized MR-based biomarker of tissue fat concentration. J Magn Reson Imaging. 2012; 36(5):1011–4. DOI: 10.1002/jmri.23741 [PubMed: 22777847]

37. Hu HH, Kan HE. Quantitative proton MR techniques for measuring fat. NMR Biomed. 2013; 26(12):1609–29. DOI: 10.1002/nbm.3025 [PubMed: 24123229]

38. Reeder SB, Cruite I, Hamilton G, Sirlin CB. Quantitative assessment of liver fat with magnetic resonance imaging and spectroscopy. J Magn Reson Imaging. 2011; 34(4):729–49. DOI: 10.1002/jmri.22580 [PubMed: 21928307]

39. Franssens BT, Hoogduin H, Leiner T, van der Graaf Y, Visseren FL. Relation between brown adipose tissue and measures of obesity and metabolic dysfunction in patients with cardiovascular disease. J Magn Reson Imaging. 2017; Epub ahead of print. doi: 10.1002/jmri.25594

40. Franssens BT, Eikendal AL, Leiner T, van der Graaf Y, Visseren FL, Hoogduin JM. Reliability and agreement of adipose tissue fat fraction measurements with water-fat MRI in patients with manifest cardiovascular disease. NMR Biomed. 2016; 29(1):48–56. DOI: 10.1002/nbm.3444 [PubMed: 26620447]

41. Karampinos DC, Yu H, Shimakawa A, Link TM, Majumdar S. T(1)-corrected fat quantification using chemical shift-based water/fat separation: application to skeletal muscle. Magn Reson Med. 2011; 66(5):1312–26. DOI: 10.1002/mrm.22925 [PubMed: 21452279]

42. Liu CY, McKenzie CA, Yu H, Brittain JH, Reeder SB. Fat quantification with IDEAL gradient echo imaging: correction of bias from T(1) and noise. Magn Reson Med. 2007; 58(2):354–64. DOI: 10.1002/mrm.21301 [PubMed: 17654578]

43. Ren J, Dimitrov I, Sherry AD, Malloy CR. Composition of adipose tissue and marrow fat in humans by 1H NMR at 7 Tesla. J Lipid Res. 2008; 49(9):2055–62. DOI: 10.1194/jlr.D800010-JLR200 [PubMed: 18509197]

44. Eggers H, Brendel B, Duijndam A, Herigault G. Dual-echo Dixon imaging with flexible choice of echo times. Magn Reson Med. 2011; 65(1):96–107. DOI: 10.1002/mrm.22578 [PubMed: 20860006]

45. Shen J, Baum T, Cordes C, Ott B, Skurk T, Kooijman H, et al. Automatic segmentation of abdominal organs and adipose tissue compartments in water-fat MRI: Application to weight-loss in obesity. Eur J Radiol. 2016; 85(9):1613–21. DOI: 10.1016/j.ejrad.2016.06.006 [PubMed: 27501897]

46. Cordes C, Dieckmeyer M, Ott B, Shen J, Ruschke S, Settles M, et al. MR-detected changes in liver fat, abdominal fat, and vertebral bone marrow fat after a four-week calorie restriction in obese women. J Magn Reson Imaging. 2015; 42(5):1272–80. DOI: 10.1002/jmri.24908 [PubMed: 25865456]

47. Franz D, Karampinos DC, Rummeny EJ, Souvatzoglou M, Beer AJ, Nekolla SG, et al. Discrimination Between Brown and White Adipose Tissue Using a 2-Point Dixon Water-Fat Separation Method in Simultaneous PET/MRI. J Nucl Med. 2015; 56(11):1742–7. DOI: 10.2967/jnumed.115.160770 [PubMed: 26272809]

48. Lundstrom E, Strand R, Johansson L, Bergsten P, Ahlstrom H, Kullberg J. Magnetic resonance imaging cooling-reheating protocol indicates decreased fat fraction via lipid consumption in suspected brown adipose tissue. PLoS One. 2015; 10(4):e0126705.doi: 10.1371/journal.pone.0126705 [PubMed: 25928226]

49. Nedergaard J, Bengtsson T, Cannon B. Unexpected evidence for active brown adipose tissue in adult humans. Am J Physiol Endocrinol Metab. 2007; 293(2):E444–52. DOI: 10.1152/ajpendo.00691.2006 [PubMed: 17473055]

50. Vijgen GH, Bouvy ND, Teule GJ, Brans B, Schrauwen P, van Marken Lichtenbelt WD. Brown adipose tissue in morbidly obese subjects. PLoS One. 2011; 6(2):e17247.doi: 10.1371/journal.pone.0017247 [PubMed: 21390318]

51. Nguyen KD, Qiu Y, Cui X, Goh YP, Mwangi J, David T, et al. Alternatively activated macrophages produce catecholamines to sustain adaptive thermogenesis. Nature. 2011; 480(7375):104–8. DOI: 10.1038/nature10653 [PubMed: 22101429]

52. Raiko J, Holstila M, Virtanen KA, Orava J, Saunavaara V, Niemi T, et al. Brown adipose tissue triglyceride content is associated with decreased insulin sensitivity, independently of age and obesity. Diabetes Obes Metab. 2015; 17(5):516–9. DOI: 10.1111/dom.12433 [PubMed: 25586670]

53. Koksharova E, Ustyuzhanin D, Philippov Y, Mayorov A, Shestakova M, Shariya M, et al. The Relationship Between Brown Adipose Tissue Content in Supraclavicular Fat Depots and Insulin Sensitivity in Patients with Type 2 Diabetes Mellitus and Prediabetes. Diabetes Technol Ther. 2017; 19(2):96–102. DOI: 10.1089/dia.2016.0360 [PubMed: 28118051]

54. Shimizu I, Walsh K. The Whitening of Brown Fat and Its Implications for Weight Management in Obesity. Curr Obes Rep. 2015; 4(2):224–9. DOI: 10.1007/s13679-015-0157-8 [PubMed: 26627217]

55. Bartelt A, Bruns OT, Reimer R, Hohenberg H, Ittrich H, Peldschus K, et al. Brown adipose tissue activity controls triglyceride clearance. Nat Med. 2011; 17(2):200–5. DOI: 10.1038/nm.2297 [PubMed: 21258337]

56. van Harmelen V, Skurk T, Rohrig K, Lee YM, Halbleib M, Aprath-Husmann I, et al. Effect of BMI and age on adipose tissue cellularity and differentiation capacity in women. Int J Obes Relat Metab Disord. 2003; 27(8):889–95. DOI: 10.1038/sj.ijo.0802314 [PubMed: 12861228]

57. Yang Y, Smith DL Jr, Hu HH, Zhai G, Nagy TR. Chemical-shift water-fat MRI of white adipose depots: inability to resolve cell size differences. Int J Body Compos Res. 2013; 11(1):9–16. [PubMed: 23667321]

58. Pasarica M, Sereda OR, Redman LM, Albarado DC, Hymel DT, Roan LE, et al. Reduced adipose tissue oxygenation in human obesity: evidence for rarefaction, macrophage chemotaxis, and inflammation without an angiogenic response. Diabetes. 2009; 58(3):718–25. DOI: 10.2337/db08-1098 [PubMed: 19074987]

59. Lee JJ, Pedley A, Hoffmann U, Massaro JM, Keaney JF Jr, Vasan RS, et al. Cross-Sectional Associations of Computed Tomography (CT)-Derived Adipose Tissue Density and Adipokines: The Framingham Heart Study. J Am Heart Assoc. 2016; 5(3):e002545.doi: 10.1161/JAHA.115.002545 [PubMed: 26927600]

60. Therkelsen KE, Pedley A, Rosenquist KJ, Hoffmann U, Massaro JM, Murabito JM, et al. Adipose tissue attenuation as a marker of adipose tissue quality: Associations with six-year changes in body weight. Obesity (Silver Spring). 2016; 24(2):499–505. DOI: 10.1002/oby.21337 [PubMed: 26694629]

61. Rosenquist KJ, Massaro JM, Pedley A, Long MT, Kreger BE, Vasan RS, et al. Fat quality and incident cardiovascular disease, all-cause mortality, and cancer mortality. J Clin Endocrinol Metab. 2015; 100(1):227–34. DOI: 10.1210/jc.2013-4296 [PubMed: 25226289]

62. Lee JJ, Pedley A, Hoffmann U, Massaro JM, Fox CS. Association of Changes in Abdominal Fat Quantity and Quality With Incident Cardiovascular Disease Risk Factors. J Am Coll Cardiol. 2016; 68(14):1509–21. DOI: 10.1016/j.jacc.2016.06.067 [PubMed: 27687192]
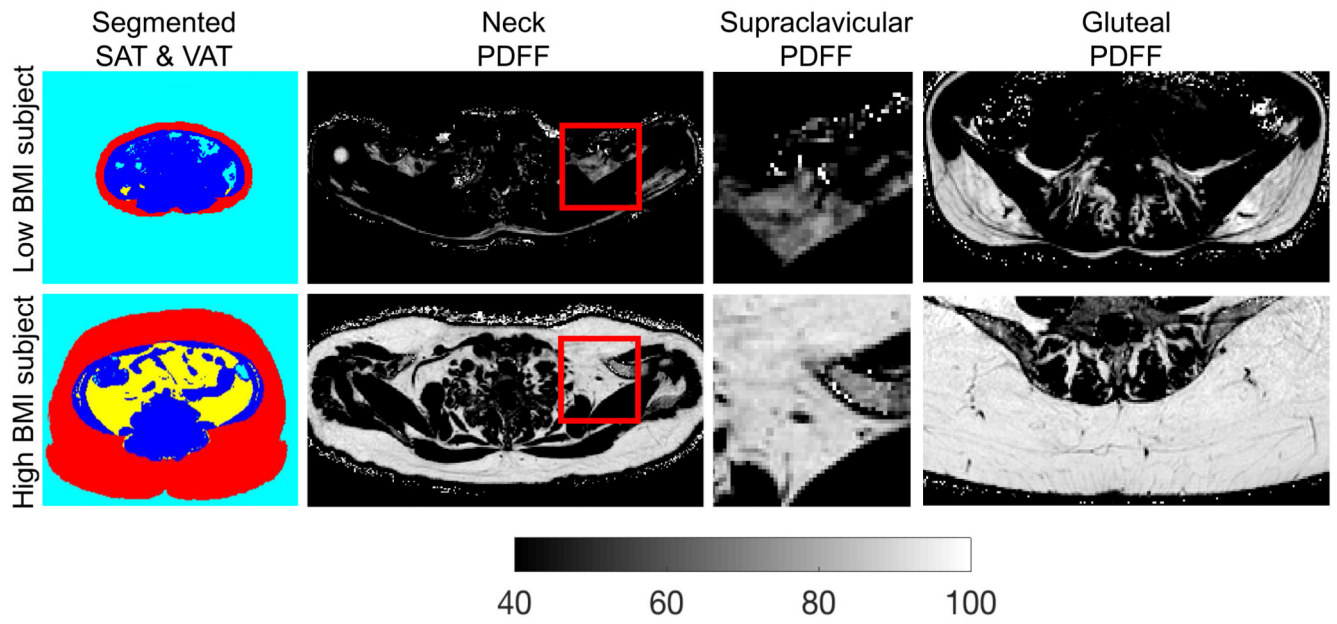
Figure 1.

Comparison of different fat depots in a low BMI female subject (first row, BMI: 17.4 kg/m^2, age = 39 years) and a high BMI female subject (second row, BMI: 38.1 kg/m^2, age = 48 years). The high BMI subject has higher SAT volume and higher VAT volume (color-coded masking using red for SAT, yellow for VAT, blue for non-adipose tissue and cyan for air on first column), higher supraclavicular PDFF (full-axial and zoomed PDFF maps on second and third columns) and higher gluteal PDFF (gluteal PDFF maps on fourth column) than the low BMI subject. PDFF: proton density fat fraction, BMI: body mass index, SAT: subcutaneous adipose tissue, VAT: visceral adipose tissue.
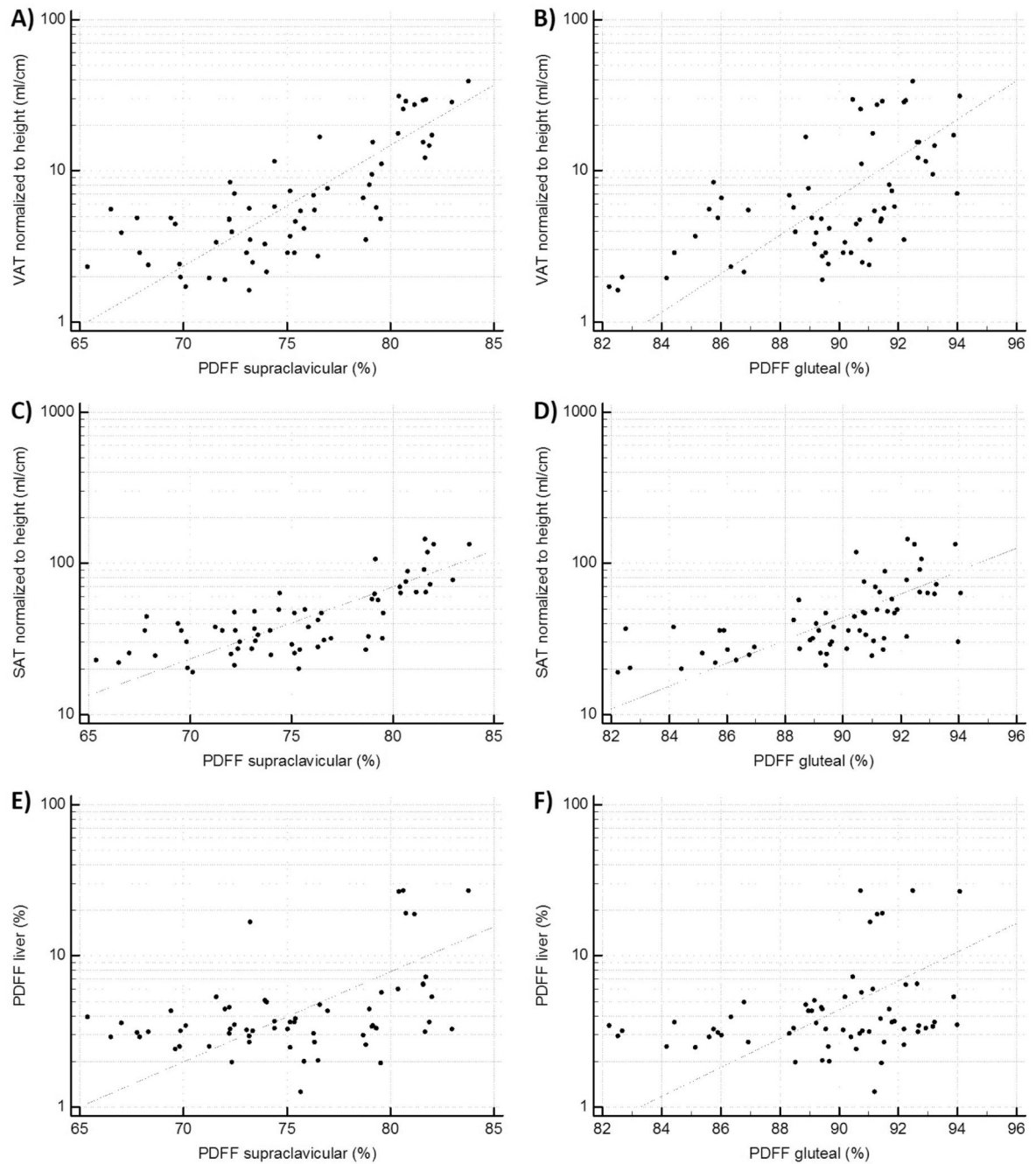
Figure 2.

Correlation analysis plots. A): Scatter plot of the correlation analysis of PDFF supraclavicular and VAT (r=0.76, p<0.0001). B): Scatter plot of the correlation analysis of PDFF gluteal and VAT (r=0.59, p<0.0001). C): Scatter plot of the correlation analysis of PDFF supraclavicular and SAT (r=0.73, p<0.0001). D): Scatter plot of the correlation analysis of PDFF gluteal and SAT (r=0.63, p<0.0001). E): Scatter plot of the correlation analysis of PDFF supraclavicular and PDFF liver (r=0.42, p=0.0008). F): Scatter plot of the

correlation analysis of PDFF gluteal and PDFF liver (r=0.30, p=0.02). PDFF: proton density fat fraction, SAT: subcutaneous adipose tissue, VAT: visceral adipose tissue.

Table 1

Characteristics of the study population. PDFF: proton density fat fraction, BMI: body mass index, SAT: subcutaneous adipose tissue, VAT: visceral adipose tissue, SD: standard deviation.

(n=61)	
Female (%)	44 (72)
Normally distributed	**Mean (SD, range)**
Weight, kg	72.3 (15.0, 52-106)
Height, cm	171.4 (9.4, 152.9-195.0)
PDFF supraclavicular, %	75.3 (4.7, 65.4-83.8)
PDFF subcutaneous gluteal, %	89.7 (2.9, 82.2-94.1)
Not normally distributed	**Median (range)**
Age, y	29.3 (21-68)
BMI, kg/m^2	23.6 (17.4-39.1)
SAT volume (normalized to height), ml/cm	37.0 (19.0-143.1)
VAT volume (normalized to height), ml/cm	5.4 (1.6-39)
Waist circumference, cm	82.0 (72-119)
Waist-to-height-ratio	0.49 (0.42-0.76)
PDFF liver, %	3.5 (1.3-27)

Table 2

Correlations of supraclavicular and gluteal PDFF with volumes of VAT and SAT as well as with liver PDFF (n=61), adjusted for age and sex and divided into age groups <30 years (n=31) and   30 years (n=30). PDFF: proton density fat fraction, SAT: subcutaneous adipose tissue, VAT: visceral adipose tissue.

Parameter	Age group	Supraclavicular PDFF (%)	Gluteal PDFF (%)
VAT volume (ml/cm)	All	r=0.76 p<0.0001	r=0.59 p<0.0001
	Adjusted*	r=0.73 p<0.0001	r=0.70 p<0.0001
	<30 years	r=0.52 p=0.003	r=0.65 p=0.0001
	30 years	r=0.82 p<0.0001	r=0.66 p=0.0001
SAT volume (ml/cm)	All	r=0.73 p<0.0001	r=0.63 p<0.0001
	Adjusted*	r=0.69 p<0.0001	r=0.60 p<0.0001
	<30 years	r=0.57 p=0.0008	r=0.54 p=0.002
	30 years	r=0.79 p<0.0001	r=0.75 p<0.0001
Liver PDFF (%)	All	r=0.42 p=0.0008	r=0.30 p=0.02
	Adjusted*	r=0.32 p=0.01	r=0.29 p=0.02
	<30 years	r=0.11 p=0.53	r=0.15 p=0.42
	30 years	r=0.47 p=0.009	r=0.41 p=0.02

*
Adjusted for age and sex.

Table 3

Correlations of supraclavicular and gluteal PDFF with anthropometric parameters (n=61), adjusted for age and sex and divided into age groups <30 years (n=31) and 30 years (n=30). PDFF: proton density fat fraction, BMI: body mass index.

Parameter	Age group	Supraclavicular PDFF (%)	Gluteal PDFF (%)
BMI (kg/m^2)	All	r=0.71 p<0.0001	r=0.47 p=0.0002
	Adjusted[*]	r=0.64 p<0.0001	r=0.48 p=0.0001
	<30 years	r=0.45 p=0.01 [†]	r=0.36 p=0.05
	30 years	r=0.81 p<0.0001 [†]	r=0.58 p=0.0007
Waist circumference (cm)	All	r=0.70 p<0.0001	r=0.45 p=0.0003
	Adjusted[*]	r=0.67 p<0.0001	r=0.54 p<0.0001
	<30 years	r=0.40 p=0.02 [†]	r=0.43 p=0.02
	30 years	r=0.79 p<0.0001 [†]	r=0.53 p=0.003
Waist-to-height ratio	All	r=0.72 p<0.0001	r=0.52 p<0.0001
	Adjusted[*]	r=0.65 p<0.0001	r=0.54 p<0.0001
	<30 years	r=0.53 p=0.002	r=0.47 p=0.007
	30 years	r=0.75 p<0.0001	r=0.63 p=0.0002

[*] Adjusted for age and sex.

[†] Significant difference between age groups (p<0.05), according to Fisher z-transformation.